Published in final edited form as:

J Am Chem Soc. 2018 December 12; 140(49): 17095–17105. doi:10.1021/jacs.8b08976.

Nanoparticles that deliver RNA to bone marrow identified by *in vivo* directed evolution

Cory D. Sago[1], **Melissa P. Lokugamage**[1], **Fatima Z. Islam**[1], **Brandon R. Krupczak**[1], **Manaka Sato**[1], and **James E. Dahlman**[1]

[1]Wallace H. Coulter Department of Biomedical Engineering, Georgia Institute of Technology, Atlanta GA, 30332, United States of America

Abstract

Bone marrow endothelial cells (BMECs) regulate their microenvironment, which includes hematopoietic stem cells. This makes BMECs an important target cell type for siRNA or gene editing (e.g., CRISPR) therapies. However, siRNA and sgRNA have not been delivered to BMECs using systemically administered nanoparticles. Given that *in vitro* nanoparticle screens have not identified nanoparticles with BMEC tropism, we developed a system to quantify how >100 different nanoparticles deliver siRNA in a single mouse. This is the first barcoding system capable of quantifying *functional cytosolic* siRNA delivery (where the siRNA drug is active), distinguishing it from *in vivo* screens that quantify biodistribution (where the drug went). Combining this approach with bioinformatics, we performed *in vivo* directed evolution, and identified BM1, a lipid nanoparticle (LNP) that delivers siRNA and sgRNA to BMECs. Interestingly, chemical analysis revealed BMEC tropism was not related to LNP size; tropism changed with the structure of poly(ethylene glycol), as well as the presence of cholesterol. These results suggest that significant changes to vascular targeting can be imparted to a LNP by making simple changes to its chemical composition, rather than using active targeting ligands. BM1 is the first nanoparticle to efficiently deliver siRNA and sgRNA to BMECs *in vivo*, demonstrating that this functional *in vivo* screen can identify nanoparticles with novel tropism *in vivo*. More generally, *in vivo* screening may help reveal the complex relationship between nanoparticle structure and tropism, thereby helping scientists understand how simple chemical changes control nanoparticle targeting.

Introduction.

siRNAs can elucidate how genes cause disease. In a typical example, a lipid nanoparticle (LNP) delivers siRNA that inhibits a target gene *in vivo*; this circumvents the need to breed inducible genetic knockout mice, which can take over a year. Nanoparticles that efficiently deliver siRNA to hepatocytes[1–3], lung and heart endothelial cells[4], and immune cells[5–8] have been used in this way. For example, a LNP with tropism to hepatocytes delivered siRNAs targeting endolysosomal genes; this uncovered how Rab5 influenced endocytosis[9]. Similar approaches have been applied to hypertension[10], heart disease[11–13], extracellular matrix

Correspondence: james.dahlman@bme.gatech.edu.

Competing interests. C.D.S., M.P.L., and J.E.D. have filed for intellectual property related to material within this publication.

signaling[14], cancer[15–16], glucose homeostasis[17], and other phenotypes[18–19]. In addition to its utility as an *in vivo* scientific reagent, siRNA has treated disease in patients. A systemically administered LNP[1] that delivers siRNA to hepatocytes halted a previously fatal disease in Phase III clinical trials[20]; clinical programs using other hepatocyte-targeting siRNA delivery systems have generated promising data as well[21].

These examples underscore the scientific and therapeutic potential of siRNAs when they can be delivered to target cells. However, most cell types cannot be targeted by systemically administered nanoparticles. Foremost amongst these is bone marrow endothelial cells (BMECs). LNPs can target lung and heart endothelial cells in mice[4], but nanoparticles have not efficiently delivered siRNA to BMECs in mice. BMECs are important target cells for several reasons. They signal to pericytes, immune cells, and hematopoietic stem cells (HSCs) in the bone marrow microenvironment[22] (Fig. 1A). By modulating the bone marrow niche, BMECs may impact heart disease[23], aging[24], and other phenotypes. Moreover, BMECs signal differently than hepatic or pulmonary endothelial cells; tissue-specific 'angiocrine' signaling is implicated in many diseases but is poorly understood[25–26]. BMECs are difficult to study in large part because manipulating gene expression *in vivo* is challenging.

A method to directly evolve LNPs with novel tropisms *in vivo* would facilitate *in vivo* studies and RNA therapies. However, most LNPs display an affinity for the liver; this is thought to be driven by physiological advantages including slow blood flow[27–28] and discontinuous vasculature in hepatic sinusoids[25]. As a result, systemically administered RNA delivery to non-liver organs remains challenging[29]. One unexplored contributor to LNP liver tropism is the process by which LNPs are selected. Like all nanoparticles, LNPs are initially tested *in vitro*, before a few lead LNPs are tested *in vivo*. However, *in vivo* LNP delivery is influenced by factors absent in cell culture[30–31]: liver / kidney / spleen / immune clearance, blood flow[27], and physical structures that disassemble nanoparticles[32]. We compared *in vitro* and *in vivo* nanoparticle biodistribution mediated by >300 LNPs and found no relationship in endothelial cells or macrophages[33]. However, *in vitro* nanoparticle delivery can predict hepatocyte delivery[34]. If *in vitro* delivery predicts hepatocyte delivery (but not endothelial cell delivery), this may help explain why LNPs selected *in vitro* target hepatocytes *in vivo*.

Testing hundreds of LNPs *in vivo* could accelerate the discovery of LNPs targeting new cell types. Our lab[33, 35–36] and others[37] have designed *in vivo* nanoparticle screens with DNA barcodes. Barcoding studies have identified liposomes for tumor delivery[37], compared *in vitro* and *in vivo* delivery[33], and uncovered how cholesterol structure influences LNP targeting. However, these studies quantify the delivery of chemotherapeutic small molecule delivery into the tumor, or alternatively, nanoparticle biodistribution. An ideal system would quantify how many LNPs functionally deliver small RNA into the cytoplasm of target cells. The distinction between nanoparticle biodistribution (where the LNP goes) and cytosolic delivery (where the RNA drug works) is crucial; over 95% of the siRNA that reaches a target cell is degraded or exocytosed[38–39]. Since endosomal escape is inefficient and cell-type dependent[40], it is difficult to predict functional delivery using biodistribution.

Here we report the first screening system capable of simultaneously quantifying how >100 LNPs functionally deliver siRNA to cells *in vivo*. We studied 160 LNPs over the course of 2 experiments, using bioinformatics to 'evolve' a LNP that targets BMECs. BMEC targeting did not depend on LNP size; instead, LNPs were targeted to BMECs by varying the chemical structure of a poly(ethylene glycol) (PEG) and the helper lipid 1,2-distearoyl-sn-glycero-3-phosphocholine (DSPC). The LNP, named BM1, is the first nanoparticle to efficiently deliver siRNA and sgRNA to BMECs *in vivo*, demonstrating that directed evolution can identify LNPs with novel tropisms.

Results.

We performed a literature search (Figure S1A) to identify nanoparticles that systemically delivered siRNA to endothelial cells in different tissues. We found multiple nanoparticles that have been reported to deliver siRNA to endothelial cells in the lung, heart, kidney, liver, lymph nodes, spleen, brain, and pancreas. An ionizable LNP named 7C1 we reported[4] was the most efficient siRNA delivery vehicle for lung, heart, and kidney endothelial cells in our search, silencing target genes by 50% after systemic siRNA doses as low as 0.02 mg / kg (Fig. 1B). No LNPs in our search targeted BMECs after systemic administration. Based on this, we synthesized the 7C1 lipid as we described[4], and investigated whether the 'original' 80: 20 formulation silenced BMECs *in vivo*. We formulated LNPs by combining the 7C1 ionizable lipid (Figure S1B) with $C_{14}PEG_{2000}$ at a molar ratio of 80: 20; the mass ratio of 7C1 and PEG to siRNA was 5:1 as reported. We injected mice with siRNA targeting Luciferase (siLuc, the control group) or ICAM-2 (siICAM-2). Both validated[4, 11–12] siRNAs were chemically modified to minimize off-target gene silencing and reduce immunostimulation (Figure S1C). We injected mice intravenously with a 1.0 mg / kg dose of siRNA, waited 3 days, isolated endothelial cells ($CD31^+CD45^-$) from bone marrow, lung, and heart using fluorescence activated cell sorting (FACS), and quantified ICAM-2 protein expression using mean fluorescent intensity (MFI) (Figure S1D). As expected, ICAM-2 protein expression was reduced in lung and heart endothelial cells isolated from mice treated with siICAM-2, relative to mice treated with the siLuc control. ICAM-2 protein expression did not change in BMECs (Fig. 1C), demonstrating the 80: 20 7C1 formulation did not target BMECs.

We hypothesized BMEC tropism could be impacted by the (i) size of the 7C1 LNP or the (ii) chemical composition of the PEG and 'helper lipids' added into the LNP. The chemical composition hypothesis was substantiated by evidence that PEG structure influences pharmacokinetics of liver-targeting LNPs *in vivo*[41]. Given that *in vitro* nanoparticle delivery to endothelial cells does not predict *in vivo* nanoparticle delivery to endothelial cells[33], we tested our hypothesis *in vivo*. We reasoned that – like AAV delivery systems - *in vivo* directed evolution could identify LNPs efficiently by refining the 'chemical space' which we were investigating (Fig. 1D). This approach has been an important advance in AAVs; directed evolution has identified viruses that deliver genes to the brain[42], eye[43], liver[44], and other tissues[45]. Refining the LNP chemical space is important; between 100 million and 200 billion chemically distinct LNPs could be formulated with validated chemistries[46].

We designed and validated a high throughput barcoding system to simultaneously quantify how >100 LNPs functionally delivered siRNA *in vivo*. This screening system is distinct from previous barcoding approaches, which quantify biodistribution (Fig. 2A). We used a validated high throughput microfluidics platform to formulate LNP-1, with chemical structure 1, so it carried siICAM-2 and barcode 1. We repeated this process N times, formulating LNP-N, with chemical structure N, to carry siICAM-2 and barcode N. The size and stability of all N LNPs was tested individually using dynamic light scattering (DLS); stable LNPs with hydrodynamic diameters between 20 and 200 nm were pooled together (other LNPs were discarded). The mass ratio of the siRNA: DNA barcode was 10:1. To identify LNPs that functionally delivered siICAM-2 into the cytoplasm, we pooled the stable LNPs together, administered them to mice intravenously, waited 3 days, and isolated ICAM-2^{Low} endothelial cells (i.e., cells with low ICAM-2 MFI) from bone marrow using FACS. We isolated and amplified the barcodes using universal primers and performed deep sequencing to identify barcode sequences that were enriched in the ICAM-2^{Low} cells (Fig. 2A). We quantified 'normalized delivery' of each barcode; normalized delivery is a calculation of the times each individual barcode is found in a sample, divided by the sum of all barcode counts in that sample (Figure S1E). Normalized delivery is analogous to counts per million in RNA-seq experiments and can be used to quantify LNP biodistribution[33, 35]. Normalized DNA delivery is different than the % dose injected / g tissue, a common parameter used to quantify nanoparticle biodistribution. Specifically, normalized delivery quantifies how efficiently a barcode was delivered, relative to all other nanoparticles tested. For example, if barcode 10 is twice as abundant as barcode 11, then we hypothesize nanoparticle 10 delivered the barcode twice as efficiently as barcode 11.

We rationally designed the DNA barcodes (Figure S1F). Specifically, we designed DNA barcodes with minimal 2° structure and G-quadruplex formation by separating our previously reported randomized 7 nucleotide region[35] into semi-randomized NWNH and NWH site. This increased DNA polymerase access during barcode amplification. We also included universal primer sites so all the barcodes were amplified with 1 set of primers (Figure S1G). The 'barcode region' of the DNA barcode was 8 nucleotides and located in the middle of the sequence. We designed the barcodes with a base distance of 3; each barcode was distinct from all other barcodes at 3 of the 8 positions. Using a QC score of 30, this reduced the odds of a 'false call' by the Illumina Sequencing machines to less than 1 / 10^9. Of the 65,536 (i.e., 4^8) potential barcode combinations, we selected 156 which would work together on Illumina sequencers. We also flanked the primer sites with 3 additional phosphorothioate-modified nucleotides to reduce exonuclease degradation.

We performed control experiments to evaluate whether co-formulating the barcode and a siRNA into the LNP would affect delivery. First, we formulated LNPs with siRNA or siRNA + barcode, and measured size with DLS; there was no difference (Figure S1H). As a second control experiment, we formulated the '80: 20' 7C1 formulation with barcodes and a control siRNA (siLuc) or barcodes and siICAM-2. Control mice were injected with 1.5 mg / kg total nucleic acid, while experimental mice were injected with a total nucleic acid dose of either 1.5, 0.5, or 0.16 mg / kg. Seventy-two hours after injection, lung endothelial cells were isolated and ICAM-2 protein expression was quantified as MFI using flow cytometry. As expected, we observed a dose-dependent increase in ICAM-2 protein silencing as the

siICAM-2 dose increased (Fig. 2B, C). We also observed an increase in the number of endothelial cells that were ICAM-2^{Low} (Fig. 2D). These data suggested that LNP-mediated delivery of siICAM-2 and barcode silenced target genes as expected *in vivo*.

To test the hypothesis that BMEC tropism was impacted by altering LNP size or LNP chemical composition of the PEG and 'helper lipids', we designed a library of LNPs consisting of 7C1, cholesterol, and 5 different lipid-PEGs (Fig. 3A, B, Figure S2A). We investigated how PEG molecular weight (2000 and 3000 Da) affected delivery; PEG molecular weight can change PEG conformation at the LNP surface, which can alter interactions between nanoparticles and the body[47]. We also varied the lipid tails in the PEG (fully saturated with 14, 16, or 18 carbons). This can change 'on / off kinetics' of PEG by altering the stability with which the hydrophilic PEG is 'anchored' into the LNP membrane[41]. Each PEG type was formulated into 24 distinct formulations with 7C1 and Cholesterol (Fig. 3C). Of the 120 LNPs formulated to carry siRNA and barcode, 115 were stable, with diameters between 20 and 200nm. These 115 LNPs were pooled together and intravenously injected at a total nucleic acid dose of 1.5 mg / kg. As a control, we compared the diameter of the pooled LNPs (53 nm) to the individual LNPs making up the pool, and found they were similar (Fig. 3D). We included 2 additional negative controls, which were 2 naked barcodes. As expected, the normalized delivery of both naked barcode controls in $ICAM2^{Low}$ BMECs was lower than the normalized delivery for all barcodes delivered by LNPs (Fig. 3E).

We tested the hypothesis that LNP size affected BMEC tropism. We plotted normalized delivery against the diameter for all 115 LNPs and observed no correlation (R^2=0.06) (Fig. 3F). To exclude the possibility these results were an artifact of testing many LNPs, we plotted normalized delivery against diameter for the top and bottom 10%; once again, we found no relationship (Fig. 3G). Finally, we plotted the size of the top and bottom 10% and found no statistical difference (Fig. 3H). Taken together, this evidence did not support our size-based hypothesis. We then tested the hypothesis that LNP chemical composition affected BMEC tropism. We analyzed the material characteristics of top performing LNPs. Specifically, we looked for material properties that were enriched in the top 10% LNPs. An example calculation (which does not include real data) for enrichment is shown in Figure S2B. In top-performing LNPs, we observed an enrichment of nanoparticles with either low (1–2.5%) or high (15–20%) PEG mole percent (Fig. 4A). Additionally, we observed that nanoparticles containing either $C_{16}PEG_{2000}$ or $C_{18}PEG_{2000}$ were enriched (Fig. 4B). To further confirm that PEG structure influenced delivery, we performed a paired analysis, comparing normalized delivery of LNPs that had identical ratios of 7C1, cholesterol, and PEG, but had either $C_{18}PEG_{2000}$ or $C_{18}PEG_{3000}$. $C_{18}PEG_{2000}$ performed significantly better compared to $C_{18}PEG_{3000}$ (Fig. 4C). Taken together, this provided preliminary evidence to support the hypothesis that LNP composition affected BMEC targeting more than size. To confirm that our screening methodology could be used to identify LNPs that functionally deliver siRNA to BMECs, we formulated the top performing LNP to carry both siLuc and siICAM-2 (Figure S2C). We intravenously injected mice with 1.0 mg / kg siRNA and measured ICAM-2 MFI on BMECs by flow cytometry. We observed a 16% reduction in ICAM-2 MFI with the winner from screen 1 (Figure S2D), which was 2.2-fold more potent (Figure S2E) than the 'original' 80:20 formulation (Fig. 1B).

To further identify LNPs with improved potency in BMECs, we designed a second LNP library that was evolved from the first; the second library was informed by our PEG enrichment data. More specifically, LNPs for library 2 were made with 7C1, cholesterol, and either $C_{16}PEG_{2000}$ or $C_{18}PEG_{2000}$. In some formulations, we also included DSPC (Fig. 5A, Figure S2F), since DSPC may improve the encapsulation of nucleic acids[48], and may alter how nanoparticles interact with serum proteins in the 'protein corona'[48]. We formulated LNPs with 20 distinct molar ratios (Fig. 5B). Of the 40 formulated, 31 formed stable nanoparticles with diameters between 20 and 200 nm. These stable LNPs were pooled together; as a control, we compared the diameter of the pooled LNPs (43 nm) to the individual LNPs, and found they were similar (Figure S2G). Pooled LNPs were administered to mice at a total nucleic acid dose of 1.5 mg / kg. Three days later, we isolated ICAM-2^{Low} BMECs using FACS, and sequenced the barcodes. We made several observations that gave us confidence in the results. The first observation was that ICAM-2 silencing in the second library was ~1.5x more robust than the first library (Fig. 5C). This suggested our second library contained more potent LNPs than the first. We noted that the experimental variance in potency of the second library was larger than the variance in the first; we analyzed mouse weight, sex, and age (Figure S2H), but were unable to come up with a specific hypothesis for this observation except for normal experimental variance *in vivo*; furthermore, the delivery of individual LNPs to ICAM-2^{Low} BMECs was consistent between technical replicates in both library 1 and 2 by paired One-way ANOVA (Figure S2I, J). Both library 1 and 2 were well tolerated (Figure S2K, L)

The second observation was that both negative controls (naked barcodes) once again had lower normalized delivery than all barcodes carried by LNPs (Fig. 5D). Third, we observed size and chemical composition results that were consistent with library 1. Specifically, we analyzed the relationship between LNP size and delivery, and observed no correlation between the size of all 31 LNPs and delivery (Fig. 5E). We did not observe any relationship between the normalized delivery and size for the top and bottom 10% (Fig. 5F), and there was no statistical difference in size between the top and bottom 10% (Fig. 5G). We next analyzed which chemical characteristics were enriched in the top 10%

of LNPs. When we analyzed LNP chemical composition, we found LNPs with high PEG percentages (15 to 20%) were enriched (Fig. 5H), as were LNPs with $C_{18}PEG_{2000}$ (Fig. 5I). Additionally, LNPs formulated with 80 mole % 7C1 (Fig. 5J), 0% DSPC (Fig. 5K), and 0.1 – 10 % cholesterol were enriched (Fig. 5L). These enrichment data suggested that a 7C1-based nanoparticle with formulation molar ratio of 80% 7C1 : 0.1–10 % cholesterol : 15 – 20% $C_{18}PEG_{2000}$ would be highly active in BMECs. We then tested the top 3 LNPs found in screen 2 (Figure S3A). Notably, all 3 reduced ICAM-2 expression in BMECs more than (i) 7C1 and (ii) the top performing LNP from screen 1 (Figure S3B).

Interestingly, we noticed that the chemical composition of the top performing individual LNP (BM1) exactly matched the enriched chemical characteristics from Figure 5 (Fig. 6A). We then selected the top performing LNP from library 2, and compared its (i) chemical composition, (ii) physical traits, (iii) *in vitro* uptake mechanism, and most importantly, (iv) ability to functionally deliver siRNA / sgRNA that manipulate BMEC gene expression *in vivo* (Fig. 6) to that of 'original' 80:20 7C1. Both 7C1 and BM1 formed stable LNPs with

diameters between 45–50 nm and had a narrow polydispersity index (PDI) (Fig. 6B). BM1 was also stable for over 10 days when stored at 4°C (Figure S3C). Additionally, the pKa of each LNP was between 6.45 and 6.55, indicating that each has a net neutral charge in blood (pH = 7.4) (Fig. 6B, Figure S3D, E), but could become cationic in early endosomes. To measure how 'original' 7C1 and BM1 are endocytosed *in vitro*, we formulated both 'original' 80:0:20 7C1 and BM1 to carry siGFP tagged with AlexaFluor647 and applied each LNP at a dose of 20 nM siRNA to Immortalized Mouse Aortic Endothelial Cells (IMAECs). iMAECs are endothelial cells that are freshly isolated from mice; they recapitulate important endothelial phenotypes[49]. After 1 hour, cells were washed and siRNA uptake was measured by flow cytometry. BM1 endocytosis was 40% less than 7C1 (Fig. 6C). When cells were pre-treated by genistein (caveolin-inhibitor) and chlorpromazine (clathrin-inhibitor), endocytosis of 7C1 decreased by at least 40%; however, BM1 endocytosis only decreased in the presence of chlorpromazine, relative to cells not treated with inhibitors (Fig. 6D, Figure S3F,G). We next tested the potency of BM1 at delivering siRNA to BMECs *in vivo*. We intravenously injected BM1 at a dose of 1 mg / kg siRNA; after 3 days, we isolated bone marrow and measured ICAM-2 MFI using flow cytometry. Compared to BMECs from mice treated with BM1 carrying siLuc, mice treated with BM1 carrying siICAM-2 showed 37% protein silencing (Fig. 6E, F). This represents a 4.8x increase in potency compared to original 7C1.

Given that we specifically evolved BM1 to target BMECs, we compared its potency to original 7C1 in lung and heart endothelial cells. We observed no difference in potency between 7C1 and BM1 in these tissues (Fig. 6G). We then quantified biodistribution of 7C1 and BM1 using QUANT, a highly sensitive ddPCR-based method[50]. Specifically, we quantified DNA barcode biodistribution in lung, heart, and bone marrow ECs, as well as $CD34^+$ hematopoietic stem and progenitor cells (HSPCs) in the bone marrow (Figure S3H,I). Biodistribution to BMECs increased 4.7x in mice treated with BM1, relative to original 7C1 formulation (Figure S3J). We did not observe significant differences in biodistribution in the other analyzed cell types. These biodistribution data were similar to the relative siRNA-mediated gene silencing we observed.

Confident that BM1 could potently deliver siRNA to BMECs, we next tested if it could also deliver sgRNA. We formulated BM1 at a dose of 1 mg / kg carrying an sgRNA targeting ICAM-2 and intravenously injected into mice constitutively expressing SpCas9[51]. This sgRNA was chemically modified with three phosphorothioates on each termini and 2'-O-methyl ribose modifications at select positions (Figure S3K)[52]. Five days after injection, we isolated BMECs and $CD34^+$ HSPCs and measured indels at ICAM-2 via Tracking Indels by Decomposition (TIDE). BM1 led to a 15% indel (insertions and deletions) rate in BMECs (Fig. 6H) and undetectable levels of indels in $CD34^+$ HSPCs (Figure S3L). BM1 was well tolerated in mice with both siRNA and sgRNA (Figure S3M, N).

Discussion

The first systemically administered siRNA therapy was approved in August 2018[20]. In this system, siRNAs are delivered to hepatocytes using an ionizable LNP[1]. This illustrates the clinical potential of RNA therapeutics and highlights the need for 'non-liver' RNA delivery

vehicles. The nanomedicine field is well positioned to make advances in non-liver delivery; thanks to important advances in nanoparticle synthesis, between 100 million and 200 billion chemically distinct nanoparticles can be formulated using available materials. However, nanoparticles must still be tested laboriously 1 by 1 *in vivo*. And as a result, most nanoparticles are only tested *in vitro*, which leaves many potential therapeutic molecules undiscovered.

Here we report that co-formulating a DNA barcode and siRNA into the same LNP can facilitate high throughput screens that quantify functional cytoplasmic siRNA delivery. This approach can help scientists in several ways. First, over the course of several experiments, it is possible to study thousands of nanoparticles deliver siRNA to any combination of cells. This could accelerate the discovery of new nanomedicines. Notably, we predict that it will eventually be feasible to study how up to 500 LNPs deliver siRNA in a single mouse. Second, we envision studies designed to systematically identify the traits that alter nanoparticle targeting directly *in vivo*. In this example, we tested two hypotheses: LNP (1) size or (2) chemical properties affect targeting. Over the course of our experiments, we consistently found no evidence to support hypothesis 1 and multiple lines of evidence to support hypothesis 2. Interestingly, our data suggested that making seemingly small changes to the LNP formulation – in our case changing the lipid tail of the PEG, and adding cholesterol - altered nanoparticle tropism. Notably, minor changes to PEG composition have altered the pharmacokinetics and function of liver-targeting LNPs[41]. However, the mechanisms mediating this effect remain unclear. In future studies, we hope to test two hypotheses. First, that PEG on / off rates in serum are altered by changing the lipid tail of the PEG. Second, that the inclusion of cholesterol alters the serum lipoproteins to which the LNP binds. It is also possible that both hypotheses are incorrect, and instead, that an yet to be discovered, multivariate effect is causing these effects. Broadly, these data suggest that LNP targeting can be altered making small changes to the chemical composition, which may offer a simple alternative[52] to traditional approaches, which rely on active targeting ligands[53–55]. These data substantiated by other recent reports[41, 56], but need to be validated in other labs. If vascular tropism can be altered by simple changes to the LNPs, then these data will be helpful by informing the number of physical and chemical variables that need to be considered when formulating chemically diverse nanoparticle libraries.

It is important to note several limitations with the current study. First, this screening system will not work with toxic or unstable nanoparticles. Second, like all DNA-based screens, it is important to include all the controls we have described herein. Third, we only used two iterative libraries; we believe future iterative libraries will be able to identify LNPs with even greater BMEC tropism. Finally, given the size of these datasets, it will be important to collaborate with ‘big data’ scientists, to understand which new, cutting edge bioinformatic approaches can be applied to these *in vivo* delivery datasets. Even with these nuances, we believe this methodology offers a solution to many technical / practical issues that impede the translation of new nanoparticles into the clinic.

Associated Content.

The following information is provided free of charge on the ACS website: Literature Review of Delivery to Endothelial Cells, Structure of 7C1, siRNA Sequences, Representative FACS Gating, Representative Normalization, Barcode Sequences, Diagram of PCR Scheme, Dynamic Light Scattering, LNP Library Chemical Composition, Enrichment Diagram, Winning LNP Confirmation, Library Diameter, Consistency of Technical Replicates, Mouse Weights, LNP Stability, LNP Ionizability, LNP Endocytosis, LNP Biodistribution, sgRNA Sequence, HSPC Indels. All data, analyses, and scripts used to generate all in the paper are available upon requests made to dahlmanlab.org.

Materials and Methods

Nanoparticle Formulation.

Nanoparticles were formulated using a microfluidic device as previously described[26]. Briefly, nucleic acids (siRNA and DNA barcodes) were diluted in citrate buffer while lipid-amine compounds, alkyl tailed PEG, cholesterol, and DSPC were diluted in ethanol. PEG, cholesterol, and DSPC was purchased from Avanti Lipids. Citrate and ethanol phases were combined in a microfluidic device by syringe pumps.

DNA Barcoding.

Each chemically distinct LNP was formulated to carry its own unique DNA barcode and siRNA. For example, LNP1 carried DNA barcode 1 and siICAM2, while the chemically distinct LNP2 carried DNA barcode 2 and siICAM2. Single stranded DNA sequences were purchased from Integrated DNA Technologies (IDT). To ensure equal amplification of each sequence, we included universal forward and reverse primer regions. Each barcode was distinguished using a unique 8 nucleotide sequence. An 8 nucleotide sequence can generate 65,536 distinct barcodes. We used 156 distinct sequences designed to prevent sequence 'bleaching' on the Illumina MiniSeq sequencing machine.

Nanoparticle Characterization.

LNP hydrodynamic diameter was measured using a plate reader formatted dynamic light scattering machine (Wyatt). LNPs were diluted in sterile 1X PBS to a concentration of ~0.06 μg/mL and analyzed. LNPs were only included if they formed monodisperse populations with diameter between 20 and 200nm. Particles that met these criteria were dialyzed with 1X phosphate buffered saline (PBS, Invitrogen), and were sterile filtered with a 0.22 μm filter.

Animal Experiments.

All animal experiments were performed in accordance with the Georgia Institute of Technology's IACUC. C57BL/6J (#000664) and constitutive SpCas9 (#026179) mice were purchased from The Jackson Laboratory and used between 5–12 weeks of age. In all experiments, we used N=3–5 mice/group. Mice were injected intravenously via the lateral tail vein. The nanoparticle concentration was determined using NanoDrop (Thermo Scientific).

Cell Isolation & Staining.

Cells were isolated 72 hours (for screens) or 120 hours (for *in vivo* gene editing) hours after injection with LNPs unless otherwise noted. Mice were perfused with 20 mL of 1X PBS through the right atrium. As we previously described[4, 33], tissues were cut and placed in a digestive enzyme solution with Collagenase Type I (Sigma Aldrich), Collagenase XI (Sigma Aldrich) and Hyaluronidase (Sigma Aldrich) at 37 °C for 45 minutes. The digestive enzyme for heart included Collagenase IX. Cell suspension was filtered through 70μm mesh and red blood cells were lysed. Cells were stained to identify populations and sorted using the BD FacsFusion in the Georgia Institute of Technology Cellular Analysis Core for *in vivo* experiments. The antibody clones used were: anti-CD31 (390, BioLegend), anti-CD102 (3C4, Biolegend), anti-CD45.2 (104, BioLegend), and anti-CD34 (SA376A4, Biolegend).

PCR Amplification for Illumina Sequencing.

All samples were amplified and prepared for sequencing using nested PCR (Supplementary Figure 1G). 2 μL of primers were added to 5 μL of Kapa HiFi 2X master mix, and 3 μL template DNA/water. The second PCR, added Nextera XT chemistry, indices and i5/i7 adapter regions. Dual-indexed samples were run on a 2% agarose gel to ensure that PCR reaction occurred before being pooled and gel purified.

Deep Sequencing.

Illumina sequencing was conducted in Georgia Institute of Technology's Molecular Evolution core. Runs were performed on an Illumina Miniseq. Primers were designed based on Nextera XT adapter sequences.

Barcode Sequencing Normalization.

Counts for each particle, per cell type, were normalized to the barcoded LNP mixture applied to cells or injected into the mouse.

TNS Assay.

The pKa of 7C1 and BM1 was measured as previously described[4]. Briefly, a stock solution of 10mM HEPES (Sigma), 10mM MES (Sigma), 10mM sodium acetate (Sigma), and 140nM sodium chloride (Sigma) was prepared and pH adjusted with hydrogen chloride and sodium hydroxide to a range of pH between 4 and 10. Using 4 replicates for each nanoparticle at each pH, 140 μL pH-adjusted buffer was added to a 96-well plate, followed by the addition 5 μL of 2-(p-toluidino)-6-napthalene sulfonic acid (60 μg / mL). 5uL of each nanoparticle was added to each well. After 5 minutes of incubation under gentle shaking, fluorescence absorbance was measured using excitation wavelengths of 325 nm and emission wavelength of 435nm.

In vitro Endocytosis.

Immortalized mouse aortic endothelial cells (IMAECs) were seeded in a 24 well plate at 40,000 cells per well and allowed to culture overnight. 7C1 and BM1 were formulated to carry Alexa647-tagged siRNA using microfluidics. After formulation, both LNPs were dialyzed for 2hrs in 1x PBS. 1 hour prior to incubation with each LNPs, inhibitors of

clathrin-mediated endocytosis (chlorpromazine, 100mM, Alfa Aesar), caveolae-mediated endocytosis (genistein, 100mM, TCI America), and macropinocytosis (5-(N-Ethyl-N-isopropyl) Amiloride, EIPA, 50mM, Toronto Research Chemicals) were added to IMAECs at a dose of 20nM siRNA / well. LNPs were left on the cells for 1 hour before the cells were washed 2x with PBS, tryspinized and prepared for flow cytometry using a BD Accuri C6.

RNA interference.

siRNAs were chemically modified at the 2' position to increase stability and negate immunostimulation. 72 hours after injection, tissues were isolated and protein expression was determined via flow cytometry. ICAM2 mean fluorescent intensity in siLuc-treated mice was normalized to 100 percent.

QUANT Biodistribution.

7C1 and BM1 LNPs were formulated to carry the DNA barcodes utilized in this study. Mice were injected at a dose of 0.5 mg / kg. After 4 hours, tissues were isolated and endothelial cells from the lung, heart, and bone marrow, as well as $CD34^+$ HSPCs were isolated by FACS. DNA barcodes were isolated using QuickExtract (Epicentre). Biodistribution was measured as previously described[50]. Briefly, the QX200™ Droplet Digital™ PCR System (Bio-Rad) was used to prep and analyze all ddPCR results. All PCR samples were prepared with 10μL ddPCR with ddPCR™ Supermix for Probes (Bio-Rad), 1μL of primer and probe mix (solution of 10μM of target probe and 20μM of Reverse/Forward Primers), 1μL of template, and 8μL water. 20μL of each reaction and 70μL of Droplet Generation Oil for Probes (Bio-Rad) were loaded into DG8™ Cartridges and covered with DG8™ Gaskets. Cartridges were placed in the QX200™ Droplet Generator to create water-oil emulsion droplets. Cycle conditions for PCR were as follows: 1 cycle of 95° for 10 minutes, followed by 40 cycles of 94°C for 30 seconds, 60°C for 1 minute, and 1 cycle of 95°C for 10 minutes. Plates were stored at 4°C until ran on the QX200™ Droplet Digital™ PCR System. For each biological rep, 2 technical repetitions were completed. In all cases, technical reps were averaged.

In vivo Cas9 Editing.

Mice constitutively expressing SpCas9 were injected with BM1 carrying 1 mg / kg of sgICAM2. sgICAM2 was modified with 2' O-methyl ribose at select positions and 3 phosphorothioates at both the 5' and 3' termini. 5 days after injection, cells were isolated via FACS. Indels were measured by TIDES.

Data Analysis & Statistics.

Sequencing results were processed using a custom R script to extract raw barcode counts for each tissue. These raw counts were then normalized with an R script prior for further analysis. Statistical analysis was done using GraphPad Prism 7; more specifically Paired 2-tail T-test or One-way ANOVAs were used where appropriate. Data is plotted as mean ± standard error mean unless otherwise stated.

Supplementary Material

Refer to Web version on PubMed Central for supplementary material.

Acknowledgments.

The authors thank M.G. Finn, Jordan E. Cattie and Anton V. Bryksin for their help. J.E.D. thanks Taylor E. Shaw.

Funding. C.D.S., M.P.L., and J.E.D. were funded by Georgia Tech startup funds (awarded to J.E.D.). C.D.S. was funded by the NIH-sponsored Research Training Program in Immunoengineering (T32EB021962). Research was funded by the Cystic Fibrosis Research Foundation (DAHLMA15XX0, awarded to J.E.D.), the Parkinson's Disease Foundation (PDF-JFA-1860, awarded to J.E.D.), the Bayer Hemophilia Awards Program (AGE DTD, awarded to J.E.D.), and the National Institutes of Health (R01DE026941, awarded to J.E.D.). This content is solely the responsibility of the authors and does not necessarily represent the official views of the National Institutes of Health.

Citations

1. Semple SC; Akinc A; Chen J; Sandhu AP; Mui BL; Cho CK; Sah DW; Stebbing D; Crosley EJ; Yaworski E; Hafez IM; Dorkin JR; Qin J; Lam K; Rajeev KG; Wong KF; Jeffs LB; Nechev L; Eisenhardt ML; Jayaraman M; Kazem M; Maier MA; Srinivasulu M; Weinstein MJ; Chen Q; Alvarez R; Barros SA; De S; Klimuk SK; Borland T; Kosovrasti V; Cantley WL; Tam YK; Manoharan M; Ciufolini MA; Tracy MA; de Fougerolles A; MacLachlan I; Cullis PR; Madden TD; Hope MJ, Rational design of cationic lipids for siRNA delivery. Nat Biotechnol 2010, 28 (2), 172–6. [PubMed: 20081866]

2. Love KT; Mahon KP; Levins CG; Whitehead KA; Querbes W; Dorkin JR; Qin J; Cantley W; Qin LL; Racie T; Frank-Kamenetsky M; Yip KN; Alvarez R; Sah DW; de Fougerolles A; Fitzgerald K; Koteliansky V; Akinc A; Langer R; Anderson DG, Lipid-like materials for low-dose, in vivo gene silencing. Proceedings of the National Academy of Sciences of the United States of America 2010, 107 (5), 1864–9. [PubMed: 20080679]

3. Dong Y; Love KT; Dorkin JR; Sirirungruang S; Zhang Y; Chen D; Bogorad RL; Yin H; Chen Y; Vegas AJ; Alabi CA; Sahay G; Olejnik KT; Wang W; Schroeder A; Lytton-Jean AK; Siegwart DJ; Akinc A; Barnes C; Barros SA; Carioto M; Fitzgerald K; Hettinger J; Kumar V; Novobrantseva TI; Qin J; Querbes W; Koteliansky V; Langer R; Anderson DG, Lipopeptide nanoparticles for potent and selective siRNA delivery in rodents and nonhuman primates. Proceedings of the National Academy of Sciences of the United States of America 2014, 111 (11), 3955–60. [PubMed: 24516150]

4. Dahlman JE; Barnes C; Khan OF; Thiriot A; Jhunjunwala S; Shaw TE; Xing Y; Sager HB; Sahay G; Speciner L; Bader A; Bogorad RL; Yin H; Racie T; Dong Y; Jiang S; Seedorf D; Dave A; Singh Sandhu K; Webber MJ; Novobrantseva T; Ruda VM; Lytton-JeanAbigail KR; Levins CG; Kalish B; Mudge DK; Perez M; Abezgauz L; Dutta P; Smith L; Charisse K; Kieran MW; Fitzgerald K; Nahrendorf M; Danino D; Tuder RM; von Andrian UH; Akinc A; Panigrahy D; Schroeder A; Koteliansky V; Langer R; Anderson DG, In vivo endothelial siRNA delivery using polymeric nanoparticles with low molecular weight. Nat Nano 2014, 9 (8), 648–655.

5. Novobrantseva TI; Borodovsky A; Wong J; Klebanov B; Zafari M; Yucius K; Querbes W; Ge P; Ruda VM; Milstein S; Speciner L; Duncan R; Barros S; Basha G; Cullis P; Akinc A; Donahoe JS; Narayanannair Jayaprakash K; Jayaraman M; Bogorad RL; Love K; Whitehead K; Levins C; Manoharan M; Swirski FK; Weissleder R; Langer R; Anderson DG; de Fougerolles A; Nahrendorf M; Koteliansky V, Systemic RNAi-mediated Gene Silencing in Nonhuman Primate and Rodent Myeloid Cells. Mol Ther Nucleic Acids 2012, 1, e4. [PubMed: 23344621]

6. Leuschner F; Dutta P; Gorbatov R; Novobrantseva TI; Donahoe JS; Courties G; Lee KM; Kim JI; Markmann JF; Marinelli B; Panizzi P; Lee WW; Iwamoto Y; Milstein S; Epstein-Barash H; Cantley W; Wong J; Cortez-Retamozo V; Newton A; Love K; Libby P; Pittet MJ; Swirski FK; Koteliansky V; Langer R; Weissleder R; Anderson DG; Nahrendorf M, Therapeutic siRNA silencing in inflammatory monocytes in mice. Nat Biotechnol 2011, 29 (11), 1005–10. [PubMed: 21983520]

7. Kedmi R; Veiga N; Ramishetti S; Goldsmith M; Rosenblum D; Dammes N; Hazan-Halevy I; Nahary L; Leviatan-Ben-Arye S; Harlev M; Behlke M; Benhar I; Lieberman J; Peer D, A modular platform for targeted RNAi therapeutics. Nat Nanotechnol 2018, 13 (3), 214–219. [PubMed: 29379205]
8. Ramishetti S; Kedmi R; Goldsmith M; Leonard F; Sprague AG; Godin B; Gozin M; Cullis PR; Dykxhoorn DM; Peer D, Systemic Gene Silencing in Primary T Lymphocytes Using Targeted Lipid Nanoparticles. ACS nano 2015, 9 (7), 6706–16. [PubMed: 26042619]
9. Zeigerer A; Gilleron J; Bogorad RL; Marsico G; Nonaka H; Seifert S; Epstein-Barash H; Kuchimanchi S; Peng CG; Ruda VM; Del Conte-Zerial P; Hengstler JG; Kalaidzidis Y; Koteliansky V; Zerial M, Rab5 is necessary for the biogenesis of the endolysosomal system in vivo. Nature 2012, 485 (7399), 465–70. [PubMed: 22622570]
10. White K; Lu Y; Annis S; Hale AE; Chau BN; Dahlman JE; Hemann C; Opotowsky AR; Vargas SO; Rosas I; Perrella MA; Osorio JC; Haley KJ; Graham BB; Kumar R; Saggar R; Saggar R; Wallace WD; Ross DJ; Khan OF; Bader A; Gochuico BR; Matar M; Polach K; Johannessen NM; Prosser HM; Anderson DG; Langer R; Zweier JL; Bindoff LA; Systrom D; Waxman AB; Jin RC; Chan SY, Genetic and hypoxic alterations of the microRNA-210-ISCU1/2 axis promote iron-sulfur deficiency and pulmonary hypertension. EMBO Mol Med 2015, 7 (6), 695–713. [PubMed: 25825391]
11. Sager HB; Dutta P; Dahlman JE; Hulsmans M; Courties G; Sun Y; Heidt T; Vinegoni C; Borodovsky A; Fitzgerald K; Wojtkiewicz GR; Iwamoto Y; Tricot B; Khan OF; Kauffman KJ; Xing Y; Shaw TE; Libby P; Langer R; Weissleder R; Swirski FK; Anderson DG; Nahrendorf M, RNAi targeting multiple cell adhesion molecules reduces immune cell recruitment and vascular inflammation after myocardial infarction. Science translational medicine 2016, 8 (342), 342ra80–342ra80.
12. Sager HB; Hulsmans M; Lavine KJ; Moreira MB; Heidt T; Courties G; Sun Y; Iwamoto Y; Tricot B; Khan OF; Dahlman JE; Borodovsky A; Fitzgerald K; Anderson DG; Weissleder R; Libby P; Swirski FK; Nahrendorf M, Proliferation and Recruitment Contribute to Myocardial Macrophage Expansion in Chronic Heart Failure. Circ Res 2016, 119 (7), 853–64. [PubMed: 27444755]
13. Budatha M; Zhang J; Zhuang ZW; Yun S; Dahlman JE; Anderson DG; Schwartz MA, Inhibiting Integrin alpha5 Cytoplasmic Domain Signaling Reduces Atherosclerosis and Promotes Arteriogenesis. Journal of the American Heart Association 2018, 7 (3) DOI: 10.1161/JAHA.117.007501.
14. Yun S; Budatha M; Dahlman JE; Coon BG; Cameron RT; Langer R; Anderson DG; Baillie G; Schwartz MA, Interaction between integrin alpha5 and PDE4D regulates endothelial inflammatory signalling. Nat Cell Biol 2016, 18 (10), 1043–53. [PubMed: 27595237]
15. Yu D; Khan OF; Suva ML; Dong B; Panek WK; Xiao T; Wu M; Han Y; Ahmed AU; Balyasnikova IV; Zhang HF; Sun C; Langer R; Anderson DG; Lesniak MS, Multiplexed RNAi therapy against brain tumor-initiating cells via lipopolymeric nanoparticle infusion delays glioblastoma progression. Proceedings of the National Academy of Sciences of the United States of America 2017, 114 (30), E6147–e6156. [PubMed: 28696296]
16. Xue W; Dahlman JE; Tammela T; Khan OF; Sood S; Dave A; Cai W; Chirino LM; Yang GR; Bronson R; Crowley DG; Sahay G; Schroeder A; Langer R; Anderson DG; Jacks T, Small RNA combination therapy for lung cancer. Proceedings of the National Academy of Sciences 2014, 111 (34), E3553–E3561.
17. Neumann UH; Ho JSS; Chen S; Tam YYC; Cullis PR; Kieffer TJ, Lipid nanoparticle delivery of glucagon receptor siRNA improves glucose homeostasis in mouse models of diabetes. Molecular metabolism 2017, 6 (10), 1161–1172. [PubMed: 29031717]
18. Chen PY; Qin L; Barnes C; Charisse K; Yi T; Zhang X; Ali R; Medina PP; Yu J; Slack FJ; Anderson DG; Kotelianski V; Wang F; Tellides G; Simons M, FGF regulates TGF-beta signaling and endothelial-to-mesenchymal transition via control of let-7 miRNA expression. Cell Rep 2012, 2 (6), 1684–96. [PubMed: 23200853]
19. Koga J; Nakano T; Dahlman JE; Figueiredo JL; Zhang H; Decano J; Khan OF; Niida T; Iwata H; Aster JC; Yagita H; Anderson DG; Ozaki CK; Aikawa M, Macrophage Notch Ligand Delta-Like 4 Promotes Vein Graft Lesion Development: Implications for the Treatment of Vein Graft Failure. Arteriosclerosis, thrombosis, and vascular biology 2015, 35 (11), 2343–53.

20. Adams D; Gonzalez-Duarte A; O'Riordan WD; Yang CC; Ueda M; Kristen AV; Tournev I; Schmidt HH; Coelho T; Berk JL; Lin KP; Vita G; Attarian S; Plante-Bordeneuve V; Mezei MM; Campistol JM; Buades J; Brannagan TH 3rd; Kim BJ; Oh J; Parman Y; Sekijima Y; Hawkins PN; Solomon SD; Polydefkis M; Dyck PJ; Gandhi PJ; Goyal S; Chen J; Strahs AL; Nochur SV; Sweetser MT; Garg PP; Vaishnaw AK; Gollob JA; Suhr OB, Patisiran, an RNAi Therapeutic, for Hereditary Transthyretin Amyloidosis. N Engl J Med 2018, 379 (1), 11–21. [PubMed: 29972753]
21. Pasi KJ; Rangarajan S; Georgiev P; Mant T; Creagh MD; Lissitchkov T; Bevan D; Austin S; Hay CR; Hegemann I; Kazmi R; Chowdary P; Gercheva-Kyuchukova L; Mamonov V; Timofeeva M; Soh CH; Garg P; Vaishnaw A; Akinc A; Sorensen B; Ragni MV, Targeting of Antithrombin in Hemophilia A or B with RNAi Therapy. N Engl J Med 2017, 377 (9), 819–828. [PubMed: 28691885]
22. Morrison SJ; Scadden DT, The bone marrow niche for haematopoietic stem cells. Nature 2014, 505 (7483), 327–34. [PubMed: 24429631]
23. Du F; Zhou J; Gong R; Huang X; Pansuria M; Virtue A; Li X; Wang H; Yang XF, Endothelial progenitor cells in atherosclerosis. Frontiers in bioscience (Landmark edition) 2012, 17, 2327–49. [PubMed: 22652782]
24. Poulos MG; Ramalingam P; Gutkin MC; Llanos P; Gilleran K; Rabbany SY; Butler JM, Endothelial transplantation rejuvenates aged hematopoietic stem cell function. J Clin Invest 2017, 127 (11), 4163–4178. [PubMed: 29035282]
25. Augustin HG; Koh GY, Organotypic vasculature: From descriptive heterogeneity to functional pathophysiology. Science 2017, 357 (6353).
26. Rafii S; Butler JM; Ding BS, Angiocrine functions of organ-specific endothelial cells. Nature 2016, 529 (7586), 316–25. [PubMed: 26791722]
27. Tsoi KM; MacParland SA; Ma XZ; Spetzler VN; Echeverri J; Ouyang B; Fadel SM; Sykes EA; Goldaracena N; Kaths JM; Conneely JB; Alman BA; Selzner M; Ostrowski MA; Adeyi OA; Zilman A; McGilvray ID; Chan WC, Mechanism of hard-nanomaterial clearance by the liver. Nat Mater 2016, 15 (11), 1212–1221. [PubMed: 27525571]
28. Zhang YN; Poon W; Tavares AJ; McGilvray ID; Chan WCW, Nanoparticle-liver interactions: Cellular uptake and hepatobiliary elimination. J Control Release 2016, 240, 332–348. [PubMed: 26774224]
29. Lorenzer C; Dirin M; Winkler AM; Baumann V; Winkler J, Going beyond the liver: progress and challenges of targeted delivery of siRNA therapeutics. J Control Release 2015, 203, 1–15. [PubMed: 25660205]
30. Cheng CJ; Tietjen GT; Saucier-Sawyer JK; Saltzman WM, A holistic approach to targeting disease with polymeric nanoparticles. Nat Rev Drug Discov 2015, 14 (4), 239–47. [PubMed: 25598505]
31. Blanco E; Shen H; Ferrari M, Principles of nanoparticle design for overcoming biological barriers to drug delivery. Nat Biotechnol 2015, 33 (9), 941–51. [PubMed: 26348965]
32. Zuckerman JE; Choi CHJ; Han H; Davis ME, Polycation-siRNA nanoparticles can disassemble at the kidney glomerular basement membrane. Proceedings of the National Academy of Sciences of the United States of America 2012, 109 (8), 3137–3142. [PubMed: 22315430]
33. Paunovska K; Sago CD; Monaco CM; Hudson WH; Castro MG; Rudoltz TG; Kalathoor S; Vanover DA; Santangelo PJ; Ahmed R; Bryksin AV; Dahlman JE, A Direct Comparison of in Vitro and in Vivo Nucleic Acid Delivery Mediated by Hundreds of Nanoparticles Reveals a Weak Correlation. Nano Lett 2018, 18 (3), 2148–2157. [PubMed: 29489381]
34. Whitehead KA; Dorkin JR; Vegas AJ; Chang PH; Veiseh O; Matthews J; Fenton OS; Zhang Y; Olejnik KT; Yesilyurt V; Chen D; Barros S; Klebanov B; Novobrantseva T; Langer R; Anderson DG, Degradable lipid nanoparticles with predictable in vivo siRNA delivery activity. Nature communications 2014, 5, 4277.
35. Dahlman JE; Kauffman KJ; Xing Y; Shaw TE; Mir FF; Dlott CC; Langer R; Anderson DG; Wang ET, Barcoded nanoparticles for high throughput in vivo discovery of targeted therapeutics. Proceedings of the National Academy of Sciences of the United States of America 2017, 114 (8), 2060–2065. [PubMed: 28167778]

36. Paunovska K; Gil CJ; Lokugamage MP; Sago CD; Sato M; Lando GN; Gamboa Castro M; Bryksin AV; Dahlman JE, Analyzing 2000 in Vivo Drug Delivery Data Points Reveals Cholesterol Structure Impacts Nanoparticle Delivery. ACS nano 2018 Doi: 10.1021/acsnano.8b03640
37. Yaari Z; da Silva D; Zinger A; Goldman E; Kajal A; Tshuva R; Barak E; Dahan N; Hershkovitz D; Goldfeder M; Roitman JS; Schroeder A, Theranostic barcoded nanoparticles for personalized cancer medicine. Nature communications 2016, 7, 13325.
38. Gilleron J; Querbes W; Zeigerer A; Borodovsky A; Marsico G; Schubert U; Manygoats K; Seifert S; Andree C; Stoter M; Epstein-Barash H; Zhang L; Koteliansky V; Fitzgerald K; Fava E; Bickle M; Kalaidzidis Y; Akinc A; Maier M; Zerial M, Image-based analysis of lipid nanoparticle-mediated siRNA delivery, intracellular trafficking and endosomal escape. Nat Biotechnol 2013, 31 (7), 638–46. [PubMed: 23792630]
39. Wittrup A; Ai A; Liu X; Hamar P; Trifonova R; Charisse K; Manoharan M; Kirchhausen T; Lieberman J, Visualizing lipid-formulated siRNA release from endosomes and target gene knockdown. Nat Biotechnol 2015, 33 (8), 870–6. [PubMed: 26192320]
40. Sigismund S; Confalonieri S; Ciliberto A; Polo S; Scita G; Di Fiore PP, Endocytosis and signaling: cell logistics shape the eukaryotic cell plan. Physiological reviews 2012, 92 (1), 273–366. [PubMed: 22298658]
41. Mui BL; Tam YK; Jayaraman M; Ansell SM; Du X; Tam YY; Lin PJ; Chen S; Narayanannair JK; Rajeev KG; Manoharan M; Akinc A; Maier MA; Cullis P; Madden TD; Hope MJ, Influence of Polyethylene Glycol Lipid Desorption Rates on Pharmacokinetics and Pharmacodynamics of siRNA Lipid Nanoparticles. Mol Ther Nucleic Acids 2013, 2, e139. [PubMed: 24345865]
42. Deverman BE; Pravdo PL; Simpson BP; Kumar SR; Chan KY; Banerjee A; Wu WL; Yang B; Huber N; Pasca SP; Gradinaru V, Cre-dependent selection yields AAV variants for widespread gene transfer to the adult brain. Nat Biotechnol 2016, 34 (2), 204–9. [PubMed: 26829320]
43. Dalkara D; Byrne LC; Klimczak RR; Visel M; Yin L; Merigan WH; Flannery JG; Schaffer DV, In vivo-directed evolution of a new adeno-associated virus for therapeutic outer retinal gene delivery from the vitreous. Science translational medicine 2013, 5 (189), 189ra76.
44. Lisowski L; Dane AP; Chu K; Zhang Y; Cunningham SC; Wilson EM; Nygaard S; Grompe M; Alexander IE; Kay MA, Selection and evaluation of clinically relevant AAV variants in a xenograft liver model. Nature 2014, 506 (7488), 382–6. [PubMed: 24390344]
45. Chan KY; Jang MJ; Yoo BB; Greenbaum A; Ravi N; Wu WL; Sanchez-Guardado L; Lois C; Mazmanian SK; Deverman BE; Gradinaru V, Engineered AAVs for efficient noninvasive gene delivery to the central and peripheral nervous systems. Nat Neurosci 2017, 20 (8), 1172–1179. [PubMed: 28671695]
46. Lokugamage MP; Sago CD; Dahlman JE Testing thousands of nanoparticles *in vivo* using DNA barcodes. Current Opinion in Biomedical Engineering 2018, 7, 1–8. [PubMed: 30931416]
47. Perry JL; Reuter KG; Kai MP; Herlihy KP; Jones SW; Luft JC; Napier M; Bear JE; DeSimone JM, PEGylated PRINT nanoparticles: the impact of PEG density on protein binding, macrophage association, biodistribution, and pharmacokinetics. Nano Lett 2012, 12 (10), 5304–10. [PubMed: 22920324]
48. Kulkarni JA; Darjuan MM; Mercer JE; Chen S; van der Meel R; Thewalt JL; Tam YYC; Cullis PR, On the Formation and Morphology of Lipid Nanoparticles Containing Ionizable Cationic Lipids and siRNA. ACS nano 2018, 12 (5), 4787–4795. [PubMed: 29614232]
49. Ni CW; Kumar S; Ankeny CJ; Jo H, Development of immortalized mouse aortic endothelial cell lines. Vascular cell 2014, 6 (1), 7. [PubMed: 24690145]
50. Sago CD; Lokugamage MP; Lando GN; Djeddar N; Shah NN; Syed C; Bryksin AV; Dahlman JE Modifying a Commonly Expressed Endocytic Receptor Retargets Nanoparticles in Vivo. Nano Lett 2018.
51. Platt RJ; Chen S; Zhou Y; Yim MJ; Swiech L; Kempton HR; Dahlman JE; Parnas O; Eisenhaure TM; Jovanovic M; Graham DB; Jhunjhunwala S; Heidenreich M; Xavier RJ; Langer R; Anderson DG; Hacohen N; Regev A; Feng G; Sharp PA; Zhang F, CRISPR-Cas9 knockin mice for genome editing and cancer modeling. Cell 2014, 159 (2), 440–55. [PubMed: 25263330]
52. Finn JD; Smith AR; Patel MC; Shaw L; Youniss MR; van Heteren J; Dirstine T; Ciullo C; Lescarbeau R; Seitzer J; Shah RR; Shah A; Ling D; Growe J; Pink M; Rohde E; Wood KM;

Salomon WE; Harrington WF; Dombrowski C; Strapps WR; Chang Y; Morrissey DV, A Single Administration of CRISPR/Cas9 Lipid Nanoparticles Achieves Robust and Persistent In Vivo Genome Editing. Cell Rep 2018, 22 (9), 2227–2235. [PubMed: 29490262]

53. Cheng Z; Al Zaki A; Hui JZ; Muzykantov VR; Tsourkas A, Multifunctional nanoparticles: cost versus benefit of adding targeting and imaging capabilities. Science 2012, 338 (6109), 903–10. [PubMed: 23161990]
54. Kheirolomoom A; Kim CW; Seo JW; Kumar S; Son DJ; Gagnon MK; Ingham ES; Ferrara KW; Jo H, Multifunctional Nanoparticles Facilitate Molecular Targeting and miRNA Delivery to Inhibit Atherosclerosis in ApoE(−/−) Mice. ACS nano 2015, 9 (9), 8885–97. [PubMed: 26308181]
55. Muro S; Garnacho C; Champion JA; Leferovich J; Gajewski C; Schuchman EH; Mitragotri S; Muzykantov VR, Control of endothelial targeting and intracellular delivery of therapeutic enzymes by modulating the size and shape of ICAM-1-targeted carriers. Mol Ther 2008, 16 (8), 1450–8. [PubMed: 18560419]
56. Kauffman KJ; Dorkin JR; Yang JH; Heartlein MW; DeRosa F; Mir FF; Fenton OS; Anderson DG, Optimization of Lipid Nanoparticle Formulations for mRNA Delivery in Vivo with Fractional Factorial and Definitive Screening Designs. Nano Lett 2015, 15 (11), 7300–6. [PubMed: 26469188]

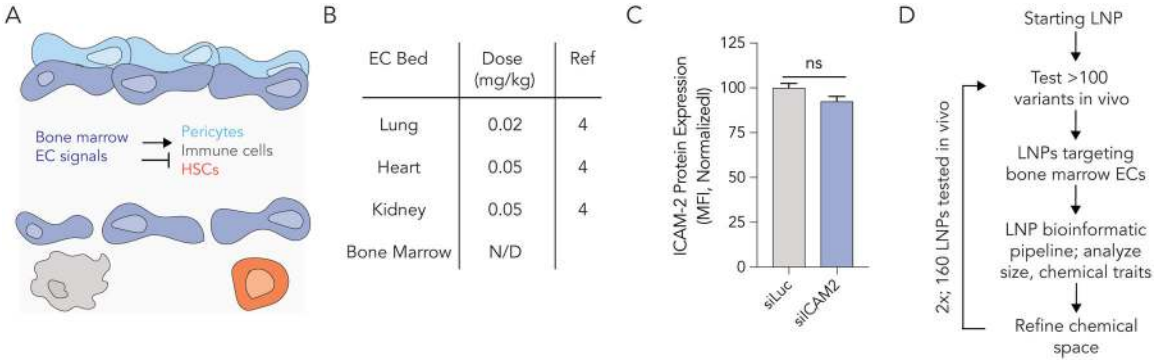

Figure 1.

Systemically delivering RNA to bone marrow endothelial cells (BMECs) is challenging. **(A)** BMECs release local signals that regulate pericytes, immune cells, and hematopoietic stem cells in the bone marrow 'niche'. **(B)** The dose (mg / kg siRNA) required to silence target gene expression in different vascular beds *in vivo*. BMECs are targeted much less efficiently than other vascular beds. **(C)** ICAM-2 protein expression after mice were treated with siLuciferase or siICAM-2 carried by the nanoparticle 7C1; the 'original 80: 20' 7C1 formulation does not deliver siRNA to BMECs. **(D)** A methodology to improve LNP delivery to BMECs; this utilizes an iterative high throughput *in vivo* screening method.

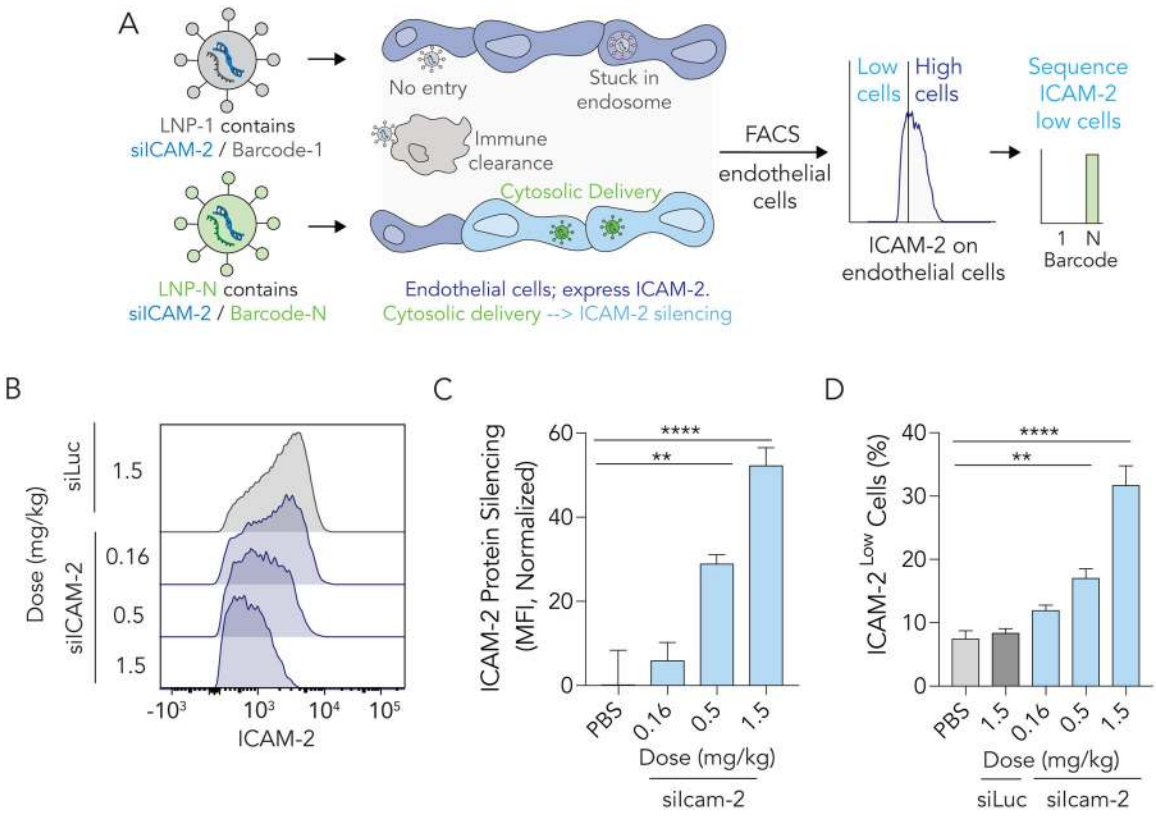

Figure 2.

Nanoparticles co-formulated with siRNA and a DNA barcode can be used to readout quantify how >100 different LNPs functionally deliver RNA into the cytoplasm of target cells in a single mouse. **(A)** Unlike previous biodistribution screens, which cannot distinguish between bound particles, particles stuck in endosomes, and particles that delivered RNA into the cytoplasm, our method identifies LNPs that functionally deliver siRNA. We do so by isolating cells that are $ICAM^{Low}$ and sequencing barcodes in those cells. **(B,C)** ICAM-2 protein expression in lung endothelial cells after mice were treated with 7C1 carrying a barcode and either siLuc or siICAM-2. ICAM-2 protein expression decreased in a dose-dependent manner. **(D)** siRNA-mediated silencing also led to a dose-dependent increase in $ICAM^{Low}$ lung endothelial cells.

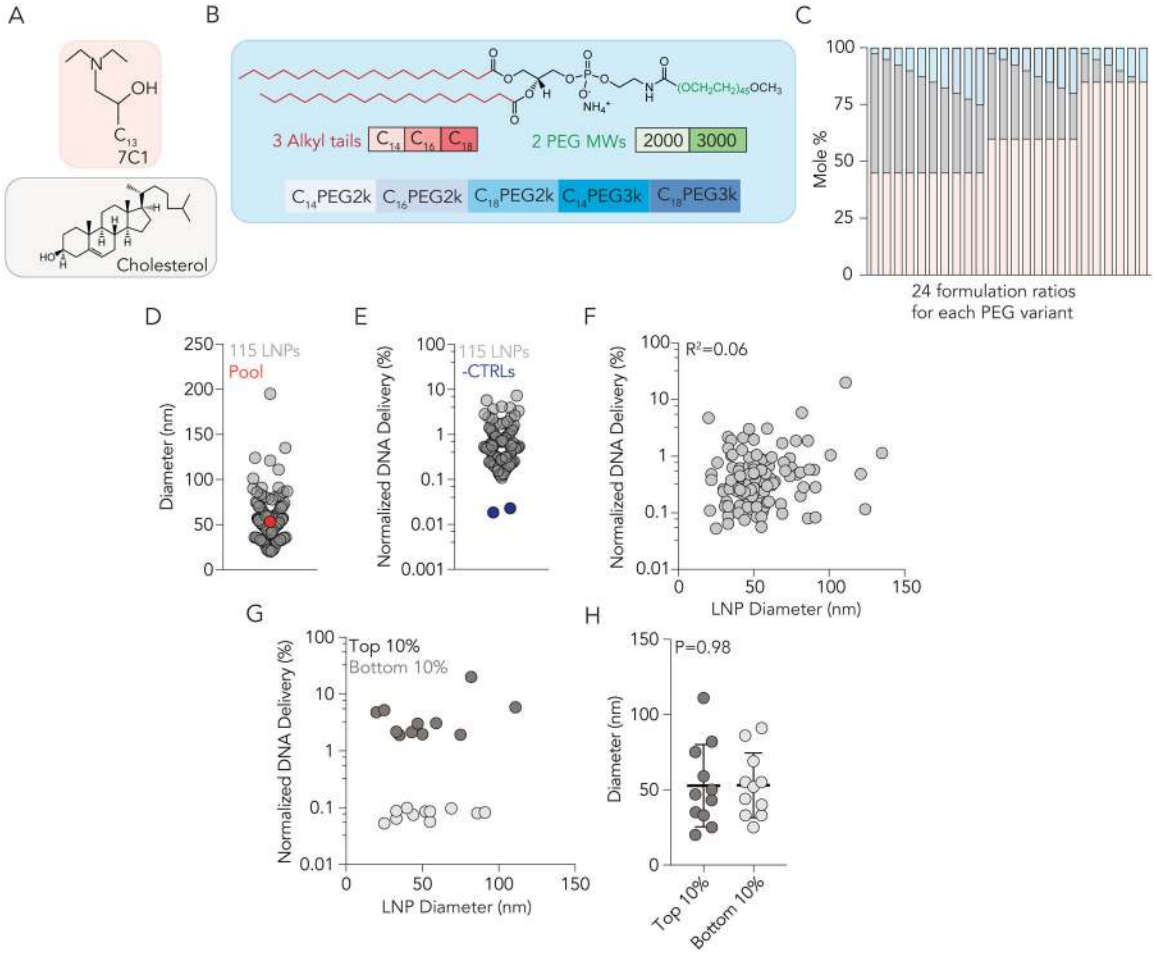

Figure 3.

The efficiency with which >100 chemically distinct LNPs delivered siRNA to cells was tested simultaneously *in vivo*. **(A)** LNPs from library 1 were made with 7C1 lipomer and cholesterol. **(B)** 5 different PEG types were used in library 1; including PEGs with 14, 16, and 18 carbon alkyl tails and molecular weights of 2000 and 3000. **(C)** 24 different formulation ratios were used for each of the 5 PEG types in library 1. **(D)** Diameter of 115 LNPs from library 1 that were pooled and injected. The diameter of the pooled library was similar to the diameter of the individual LNPs. **(E)** Normalized DNA delivery in BMECs for 115 LNPs and the 2 negative controls, which were naked. **(F)** Correlation between LNP diameter (nm) and normalized DNA delivery in BMECs for all 115 LNPs in Library 1. **(G)** Correlation between LNP diameter (nm) and normalized DNA delivery in the top and bottom 10% LNPs based on performance from library 1. **(H)** Diameter (nm) of top and bottom 10% LNPs. Taken together, the data in **(F-H)** suggest the relationship between siRNA delivery and LNP size (between 20 and 200 nm) is non-existent.

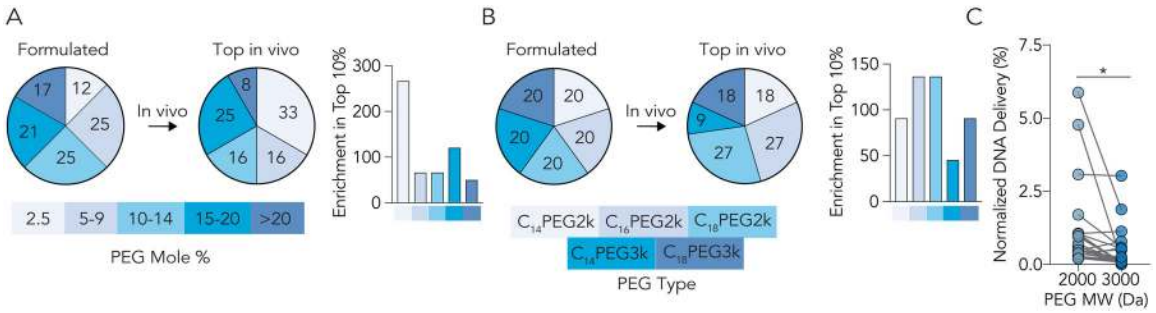

Figure 4.

LNP delivery to BMEC changes with PEG structure. **(A)** Enrichment analysis suggests that **(A)** low and high PEG Mole% as well as **(B)** C_{16}PEG2000 and C_{18}PEG2000 can promote delivery to in BMECs *in vivo*. Enrichment is described in the Supplement. **(C)** Paired comparison of LNPs with identical formulation ratios suggest that $C_{18}PEG_{2000}$ outperforms $C_{18}PEG_{3000}$ promotes BMEC targeting *in vivo* ($P<0.05$, Paired 2-tail T-Test).

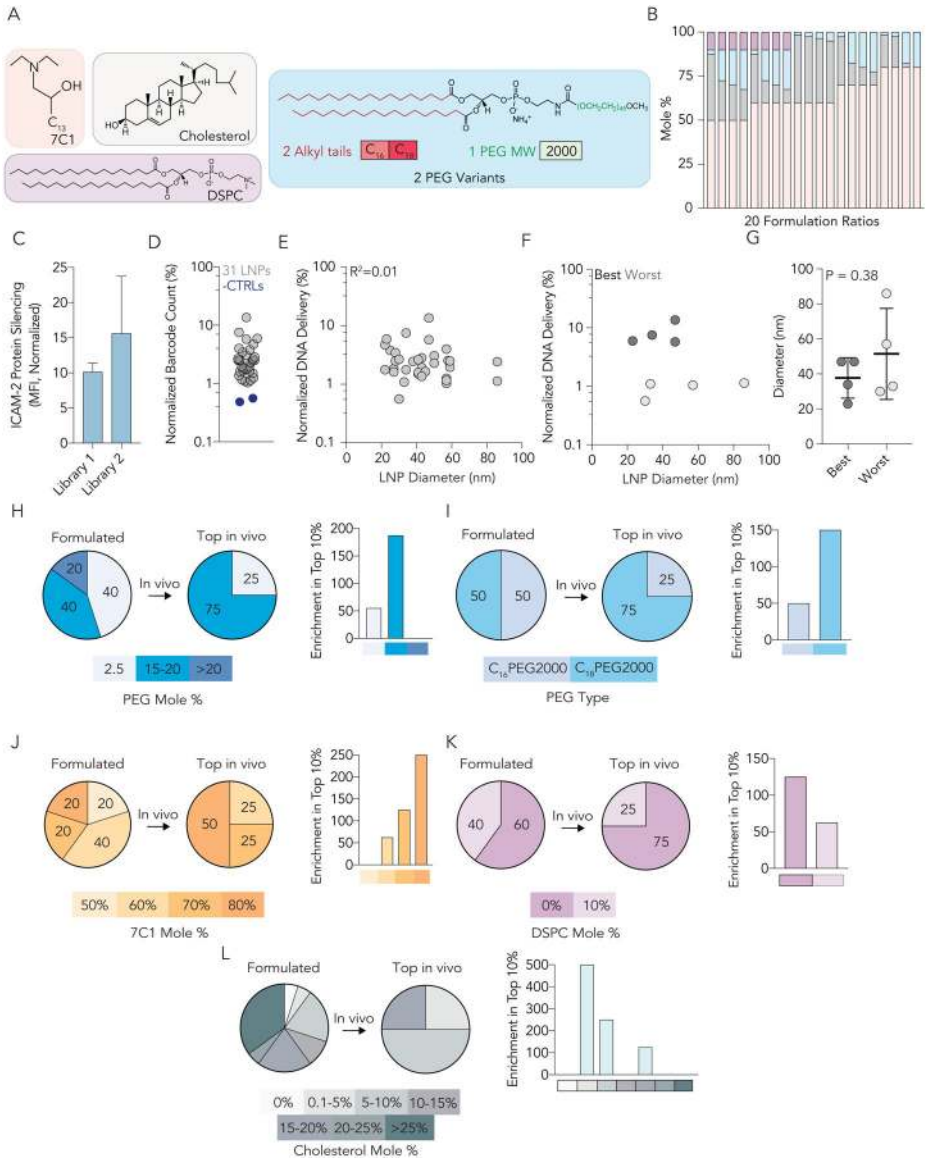

Figure 5.

Analysis of LNP size and chemical traits from a second library further suggests BMEC targeting is influenced by LNP chemical composition. **(A)** LNPs from library 2 were made with 7C1 lipomer, cholesterol, and DSPC. **(B)** Two different PEG types were used in library 2 - $C_{16}PEG_{2000}$ and $C_{18}PEG_{2000}$. These structures were selected based on data from LNP library 1. **(C)** 20 different formulation ratios were used for each of the two PEG types in library 2. **(D)** ICAM-2 protein silencing in BMECs 3 days after mice were injected with the library of LNPs at a total dose of 1.5 mg / kg. Notably, ICAM-2 silencing was more potent in BMECs than library 1. **(D)** Normalized DNA delivery in BMECs for 31 LNPs and 2 naked barcodes; as expected the naked barcodes performed poorly. **(E)** Correlation between LNP diameter (nm) and normalized DNA delivery in BMECs for all 31 LNPs in Library 2. **(F)** Correlation between LNP diameter (nm) and normalized DNA delivery in the top and bottom 10% LNPs based on performance from library 2. **(G)** Diameter (nm) of top and

bottom 10% LNPs. Taken together, **(E-G)** further suggest BMEC targeting is not influenced by LNP size between 20 and 200 nm. **(H)** Enrichment of LNPs containing PEG Mole % between 15–20% in BMECs *in vivo*. **(I)** Enrichment of LNPs containing C_{18}PEG2000 in BMECs *in vivo*. **(J)** Enrichment of LNPs containing 80 mole % 7C1 in BMECs *in vivo*. **(K)** Enrichment of LNPs containing 0 mole % DSPC in BMECs *in vivo*. **(L)** Enrichment of LNPs containing 0.1 – 10 mole % cholesterol in BMECs *in vivo*.

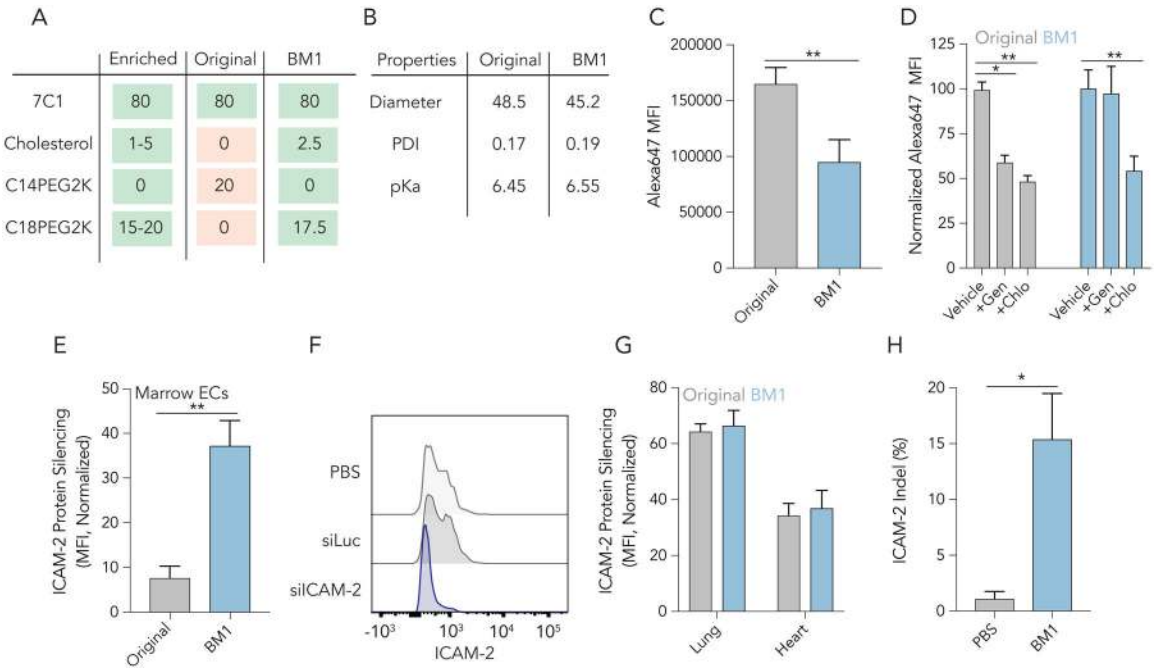

Figure 6.

Comparing BM1 and the original 80: 20 7C1 formulation reveal differences in nanoparticle behavior. **(A)** A table of the chemical properties enriched by the *in vivo* screens, the original 7C1 formulation, and BM1. Notably, BM1 has all the properties that were enriched in BMECs selected from LNP library 2. **(B)** Diameter, polydispersity index, and pKa for original 7C1 and BM1. There are no significant differences between the formulations. **(C)** *In vitro* uptake of 7C1 and BM1 *in vitro* quantified as Alexa647 MFI 1 hour after immortalized aortic endothelial cells were treated with fluorescent LNPs. The original formulation is **(D)** is inhibited by the endocytosis inhibitors genistein (caveolin) and chlorpromazine (clathrin), whereas BM1 uptake is only inhibited by chlorpromazine. **(E)** ICAM-2 protein silencing in BMECs 3 days after mice were treated with siLuc carried by original 7C1 or BM1. BM1 delivered siICAM-2 to BMECs much more efficiently than 7C1 ($P<0.01$, Unpaired 2-tail T-test) **(F)** Histogram of ICAM-2 protein expression in BMECs following the administration of PBS or BM1 carrying siLuc or siICAM-2 at 1 mg / kg. **(G)** ICAM-2 protein silencing mediated by a 1.0 mg / kg injection of 7C1 and BM1 in lung and heart endothelial cells. After evolving BM1 to target bone marrow, we did not observe any increased potency in lung or heart EC delivery. **(H)** The percentage of BMEC loci with targeted insertions or deletions (indels, i.e., mutations) after BM1 was formulated with another small RNA (sgICAM-2) and injected into Cas9 mice at a dose of 1 mg / kg.